Impact excitation of the $n=2$ fine-structure levels in hydrogenlike ions by protons and electrons

B. Zygelman and A. Dalgarno
Harvard-Smithsonian Center for Astrophysics, 60 Garden Street, Cambridge, Massachusetts 02138
(Received 6 October 1986)

Quantal close-coupling calculations of the impact excitation of the $n=2$ fine-structure levels in the hydrogenlike ions Ar^{17+}, S^{15+}, Mg^{11+}, C^{5+}, and He^{+} by protons and electrons are presented, and the resulting cross sections and rate coefficients are compared with previous values. The effects of relativity on the proton-impact excitation cross sections for ions with high nuclear charge are investigated. Plasma-density effects on the transition cross sections are explored using a Debye-screening model, and it is shown that the screening of the ion alters the excitation cross sections substantially and brings the ratio of the cross sections towards the statistical value. The calculated transition rates are used to model the ratio of the intensities of the two components of Ly-α radiation emitted by impurity hydrogenlike ions in an optically thin, hydrogen plasma. The results confirm that at intermediate plasma densities proton-impact-induced transitions redistribute the $n=2$ fine-structure-level population ratio away from the statistical value.

I. INTRODUCTION

Observations[1] of Lyman-α radiation emitted by Mg^{11+} ions in solar flares show deviations of the intensity ratio, $\beta=I(2p_{1/2}\text{-}1s_{1/2})/I(2p_{3/2}\text{-}1s_{1/2})$, from the statistical value of one-half. Similar deviations in β have been observed from radiation emitted by impurity S^{15+} ions in the Alcator Tokamak[2] and by other hydrogenlike ions in laser-produced plasmas.[3]

In a plasma that is sufficiently dense, collisional excitations of the fine-structure levels of the ions drive the populations of the levels toward a Boltzmann distribution, and the β ratio is effectively determined by the statistical weights of the levels. At the other extreme, of low plasma densities, the populations of the excited levels in the ions are governed by radiative captures followed by radiative emission to the ground state and β again has the statistical value. In the intermediate-density region, the probability that the ion undergoes a transition from one fine-structure level to another due to collisions with plasma constituents becomes comparable with the probability that the ion radiates a Lyman-α photon. In this region the fine-structure-level populations may differ from their statistical values, and the value of β could prove to be a valuable diagnostic probe of the plasma environment.

Theoretical studies by Vinogradov *et al.*[4] of β for radiation emitted by hydrogenlike ions in optically thin laser-produced plasmas predicted β to differ significantly from the statistical value over a wide range of plasma densities, and they suggested that ion-ion collisions are primarily responsible for redistributing the fine-structure populations away from their statistical values. Beigman *et al.*[5] calculated β for the impurity hydrogenlike ions seen in the solar corona, and found that it departed from the statistical value over a wide range of plasma densities. Further, more comprehensive analyses of the coronal plasma by Ljepojevic *et al.*[6] yielded the same qualitative functional dependence of β on the plasma density and temperature.

In modeling β, various approximations are employed to obtain the collision rates of the fine-structure transitions. Among them are the Born approximation with a model potential,[4,7,8] the Coulomb-Born approximation,[7] a unitarized Coulomb-Born approximation,[8,9] and semiclassical methods.[5,6] In this paper we carry out fully quantal close-coupling calculations of the proton- and electron-impact excitation rates for transitions within the $n=2$ fine-structure levels of the ions He^{+}, C^{5+}, Mg^{11+}, S^{15+}, and Ar^{17+}. Scaling arguments can be used to predict the fine-structure excitation rate coefficients for the entire range of hydrogenlike ions with nuclear charges $2\leq Z\leq 18$.

In Sec. II we present the scattering formalism. We perform a close-coupling expansion of the scattering amplitude over a set of atomic target states that contain all states within the $n=2$ manifold. The expansion should be adequate for proton-ion collisions for values of nuclear charge $Z>2$ because the Coulomb repulsion between the scattering partners inhibits close encounters. In the case of proton-He^{+} collisions, molecular effects may be significant and our results are less reliable. We use the same formalism to calculate electron-impact excitation cross sections. At impact energies far above the fine-structure thresholds, the majority of the contribution to the total cross section comes from partial waves corresponding to large impact parameters and contributions due to exchange forces are negligible. Near threshold, our calculated cross sections are less accurate but we are concerned here with plasmas for which the electron temperature is much larger than the threshold temperature.

The close-coupling equations are expressed as a set of coupled radial equations for the scattering amplitude at each value of the total angular momentum J of the projectile-target system. The long-range coupling for the dipole-allowed transitions causes a significant contribution to the total cross section from very large values of J. For large J, numerical solution of the radial equations be-

comes prohibitive, but we may use the unitarized Coulomb-Born approximation to get accurate partial cross sections.

Relativistic effects are important for ions with large nuclear charge. We examine the modifications necessary in our close-coupling equations when the ion target states are represented by fully relativistic four-component wave functions.

In a very hot dense plasma, the proton- and electron-ion interactions are screened by the surrounding plasma environment. They can be described approximately by a Debye-Hückel potential.[10,11] We present calculations for the impact excitation of Ar^{17+} when the long-range potentials are replaced by short-range Debye-Hückel potentials with various values of the Debye parameter. Finally, the calculated excitation rate coefficients are used to model the Lyman-α line intensities from photons emitted by the impurity ions He^{+}, C^{5+}, Mg^{11+}, S^{15+}, and Ar^{17+} in optically thin, hydrogen-based plasmas.

II. FORMALISM

We consider a particle with charge q scattered by a hydrogenlike ion with nuclear charge Z (atomic units are implicit, unless otherwise stated). The Hamiltonian in the center-of-mass frame is given by

$$H_T=-\frac{1}{2\mu}\nabla_R^2+H(\mathbf{r})+\frac{Zq}{R}-\frac{q}{|\mathbf{R}-\mathbf{r}|}\ , \tag{1}$$

where $\mathbf{R}$ is the coordinate of the scattered particle, $\mathbf{r}$ is the coordinate of the bound electron, μ is the reduced mass of the system, and $H(\mathbf{r})$ is the Hamiltonian for the bound atomic electron. It is assumed that transitions among the atomic levels of the ion are induced by the interaction $-q/|\mathbf{R}-\mathbf{r}|$. We restrict attention to transitions within the $2p_{1/2}$, $2p_{3/2}$, and $2s_{1/2}$ fine-structure levels. In order to obtain the scattering matrix for these transitions, we must solve Eq. (1) within some appropriate approximation and match the solution to the boundary condition for scattering in the asymptotic region. We solve (1) by utilizing a close-coupling expansion of the wave function over a set of channel states $|\Gamma\rangle$. The outgoing wave function for the system, originally prepared in state Γ', is given by

$$\Psi_{\Gamma'}^{+}(\mathbf{R},\mathbf{r})=\sum_{\Gamma}\frac{F_{\Gamma',\Gamma}(R)}{R}|\Gamma\rangle\ . \tag{2a}$$

The channel kets $|\Gamma\rangle\equiv|JMln\lambda j\rangle$ are specified by the total angular momentum and azimuthal quantum numbers J,M; the incoming particle orbital angular momentum l; the total and orbital angular momenta of the bound electron j,λ; and the radial quantum number n. We restrict the expansion to the channels with $n=2$. The Schrödinger equation for the scattering amplitudes becomes

$$\left[\frac{d^2}{dR^2}-\frac{l(l+1)}{R^2}\right]F_{\Gamma',\Gamma}(R)+\kappa_{nj}^2F_{\Gamma',\Gamma}(R)-2\mu\sum_{\Gamma''}\langle\Gamma|V|\Gamma''\rangle F_{\Gamma',\Gamma''}(R)=0\ , \tag{2b}$$

where

$$\kappa_{nj}^2\equiv 2\mu(E_T-\varepsilon_{nj}) \tag{2c}$$

and E_T and ε_{nj} are the total and atomic energy eigenvalues, respectively.

Because of parity conservation, the equations decouple into two independent sets of four-channel equations. The set of channel states with parity $(-1)^{J-1/2}$ is

$$\begin{aligned}&|JMJ-\tfrac{1}{2}2s_{1/2}\rangle\\&|JMJ+\tfrac{1}{2}2p_{1/2}\rangle\\&|JMJ+\tfrac{1}{2}2p_{3/2}\rangle\\&|JMJ-\tfrac{3}{2}2p_{3/2}\rangle\end{aligned} \tag{3a}$$

and the set with parity $(-1)^{J+1/2}$ is

$$\begin{aligned}&|JMJ+\tfrac{1}{2}2s_{1/2}\rangle\\&|JMJ-\tfrac{1}{2}2p_{1/2}\rangle\\&|JMJ+\tfrac{3}{2}2p_{3/2}\rangle\\&|JMJ-\tfrac{1}{2}2p_{3/2}\rangle\ .\end{aligned} \tag{3b}$$

The potential matrix $\langle\Gamma|V|\Gamma'\rangle$ is given by

$$q\left\langle JMln\lambda j\left|\frac{Z}{R}-\frac{1}{|\mathbf{R}-\mathbf{r}|}\right|j'\lambda'n'l'M'J'\right\rangle\ . \tag{4}$$

Expanding the interaction operator as a scalar product of the irreducible tensors C_k of rank k according to[12]

$$\frac{1}{|\mathbf{R}-\mathbf{r}|}=\sum_{k=0}^{\infty}\frac{r_<^k}{r_>^{k+1}}C_k(r)\cdot C_k(\mathbf{R})\ , \tag{5a}$$

we get

$$\left\langle\Gamma\left|\frac{1}{|\mathbf{R}-\mathbf{r}|}\right|\Gamma'\right\rangle=\sum_{k=0}^{\infty}(-1)^{J+j+l'}\delta_{J,J'}\delta_{M,M'}\begin{Bmatrix}l' & j' & J\\ j & l & k\end{Bmatrix}\langle l||C_k(\mathbf{R})||l'\rangle\left\langle j\lambda n\left|\left|C_k(\mathbf{r})\frac{r_<^k}{r_>^{k+1}}\right|\right|j'\lambda'n'\right\rangle\ . \tag{5b}$$

The reduced matrix elements can be expressed[12] by

$$\langle l||C_k(\mathbf{R})||l'\rangle=(-1)^l[l,l']^{1/2}\begin{pmatrix}l & k & l'\\ 0 & 0 & 0\end{pmatrix} \tag{6a}$$

and

$$\left\langle j\lambda n \left\| C_k(\mathbf{r})\frac{r_<^k}{r_>^{k+1}} \right\| j'\lambda' n' \right\rangle = (-1)^{j+1/2}[j,j']^{1/2} \begin{Bmatrix} j & k & j' \\ \frac{1}{2} & 0 & -\frac{1}{2} \end{Bmatrix} R_{n'\lambda'}^{n\lambda}(k,R) \ . \tag{6b}$$

The sole dependence of the reduced matrix element of $C_k(r)$ in (6) on the orbital angular momenta λ,λ' is through the parity-conservation requirement, $\lambda+\lambda'+k$ is an even integer, and in the radial matrix element $R_{n'\lambda'}^{n\lambda}(k,R)$. The radial matrix elements are defined as

$$R_{n'\lambda'}^{n\lambda}(k,R)=\frac{1}{R^{k+1}}\int_0^R dr\, P_{n\lambda}(r)P_{n'\lambda'}(r)r^k + R^k\int_R^\infty dr\frac{P_{n\lambda}(r)P_{n'\lambda'}(r)}{r^{k+1}} \ , \tag{7}$$

where $P_{n\lambda}(r)/r$ are the hydrogenic radial functions for the bound electron in state $n\lambda$. Combining (5b) and (6) with (4), we obtain

$$\langle \Gamma \mid V \mid \Gamma' \rangle = q\left[\delta_{\Gamma,\Gamma'}\left(\frac{Z}{R}-R_{n\lambda}^{n\lambda}(0,R)\right) - \delta_{J,J'}\delta_{M,M'}V_{l'j'\lambda'n'}^{lj\lambda n}(J,R)\right] \tag{8a}$$

where

$$V_{l'j'\lambda'n'}^{lj\lambda n}(J,R)=\sum_{k=1}^{\infty} Q_{l'j'\lambda'}^{lj\lambda}(k,J)R_{n'\lambda'}^{n\lambda}(k,R) \ , \tag{8b}$$

$$Q_{l'j'\lambda'}^{lj\lambda}(k,J)=(-1)^{J-1/2+k}\begin{Bmatrix} l' & j' & J \\ j & l & k \end{Bmatrix}\begin{Bmatrix} j & k & j' \\ \frac{1}{2} & 0 & -\frac{1}{2} \end{Bmatrix} \times \begin{Bmatrix} l & k & l' \\ 0 & 0 & 0 \end{Bmatrix}[j,j']^{1/2}[l,l']^{1/2} \ . \tag{8c}$$

Selection rules limit the multipole sum in (8b) to the dipole $k=1$, and quadrupole $k=2$, terms. The explicit representation for the angular coefficients $Q_{l'j'\lambda'}^{lj\lambda}(k,J)$ for the channel states (3a) and (3b) is presented in Table I.

Inserting the nonrelativistic hydrogenic radial wave functions,[13] $P_{n\lambda}(r)$, into the integral (7), we obtain

$$\begin{aligned} \frac{R_{20}^{20}(0,R)}{Z} &= \frac{1}{x}-e^{-x}\left(\frac{3}{4}+\frac{1}{x}+\frac{x^2}{8}+\frac{x}{4}\right), \\ \frac{R_{21}^{21}(0,R)}{Z} &= \frac{1}{x}-e^{-x}\left(\frac{1}{x}+\frac{3}{4}+\frac{x}{4}+\frac{x^2}{24}\right), \\ \frac{R_{20}^{21}(1,R)}{Z} &= \frac{9}{\sqrt{3}}\left[-\frac{1}{x^2}+e^{-x}\left(\frac{1}{2}+\frac{1}{x}+\frac{1}{x^2}+\frac{x}{6}+\frac{x^2}{24}\right)\right], \\ \frac{R_{21}^{21}(2,R)}{Z} &= \frac{30}{x^3}-e^{-x}\left(5+\frac{30}{x^2}+\frac{30}{x^3}+\frac{15}{x}+\frac{5x}{4}+\frac{5x^2}{24}\right), \end{aligned} \tag{9}$$

where the scaled coordinate $x\equiv RZ$.

The S matrix in the Γ representation is obtained by solving Eq. (2b) numerically subject to the boundary conditions,

TABLE I. Angular coupling coefficients (8c) as a function of the total angular momentum J. Entires in the first three rows are the dipole coupling coefficients; the remaining entries are the quadrupole coupling coefficients.

Parity $(-1)^{J-1/2}$ coefficients		Parity $(-1)^{J+1/2}$ coefficients	
$Q_{J+1/2,1/2,1}^{J-1/2,1/2,0}$	$\frac{1}{3}$	$Q_{J-1/2,1/2,1}^{J+1/2,1/2,0}$	$\frac{1}{3}$
$Q_{J+1/2,3/2,1}^{J-1/2,1/2,0}$	$-\left[\frac{2J+3}{36J}\right]^{1/2}$	$Q_{J+3/2,3/2,1}^{J+1/2,1/2,0}$	$-\left[\frac{2J+3}{12(J+1)}\right]^{1/2}$
$Q_{J-3/2,3/2,1}^{J-1/2,1/2,0}$	$\left[\frac{2J-1}{12J}\right]^{1/2}$	$Q_{J-1/2,3/2,1}^{J+1/2,1/2,0}$	$\left[\frac{2J-1}{36(J+1)}\right]^{1/2}$
$Q_{J+1/2,3/2,1}^{J+1/2,1/2,1}$	$-\left[\frac{2J+3}{100J}\right]^{1/2}$	$Q_{J+3/2,3/2,1}^{J-1/2,1/2,1}$	$-\left[\frac{6J+9}{100(J+1)}\right]^{1/2}$
$Q_{J-3/2,3/2,1}^{J+1/2,1/2,1}$	$\left[\frac{3(2J-1)}{100J}\right]^{1/2}$	$Q_{J-1/2,3/2,1}^{J-1/2,1/2,1}$	$\left[\frac{2J-1}{100(J+1)}\right]^{1/2}$
$Q_{J+1/2,3/2,1}^{J+1/2,3/2,1}$	$\frac{2J-3}{20J}$	$Q_{J+3/2,3/2,1}^{J+3/2,3/2,1}$	$\frac{-(2J+5)}{20(J+1)}$
$Q_{J-3/2,3/2,1}^{J+1/2,3/2,1}$	$\frac{[3(2J+3)(2J-1)]^{1/2}}{20J}$	$Q_{J-1/2,3/2,1}^{J+3/2,3/2,1}$	$\frac{[3(2J+3)(2J-1)]^{1/2}}{20(J+1)}$
$Q_{J-3/2,3/2,1}^{J-3/2,3/2,1}$	$\frac{-(2J-3)}{20J}$	$Q_{J-1/2,3/2,1}^{J-1/2,3/2,1}$	$\frac{2J+5}{20(J+1)}$

$$F_{\Gamma,\Gamma'}(R=0)=0\ ,$$
$$\lim_{R\to\infty} F_{\Gamma',\Gamma}\sim\frac{1}{k_\Gamma^{1/2}}\left[\delta_{\Gamma,\Gamma'}\sin\left[k_\Gamma R-\frac{\pi}{2}l_\Gamma-\eta_\Gamma\ln(2k_\Gamma R)+\sigma_{l_\Gamma}\right]+K_{\Gamma',\Gamma}\cos\left[k_\Gamma R-\frac{\pi}{2}l_\Gamma-\eta_\Gamma\ln(2k_\Gamma R)+\sigma_{l_\Gamma}\right]\right]\ , \tag{10a}$$

where k_Γ is the wave number for the scattered particle in channel Γ, l_Γ is the orbital angular momentum of the scattered projectile, σ_{l_Γ} is the Coulomb phase factor,[14] η_Γ is the Coulomb parameter,

$$\eta_\Gamma=\frac{(Z-1)q\mu}{k_\Gamma}\ , \tag{10b}$$

and $K_{\Gamma,\Gamma'}$ is a real symmetric matrix related to the S matrix by

$$\underline{S}=(1+i\underline{K})(1-i\underline{K})^{-1}\ . \tag{10c}$$

The transition cross section for the ion to go from state λj to λ',j' is expressed in terms of the S matrix by

$$\sigma(\lambda j\to\lambda' j')=\frac{\pi}{2\mu E(2j+1)}\times\sum_{J,l,l'}(2J+1)[\,|S_{lj\lambda}^{l'j'\lambda'}(J,A)|^2+|S_{lj\lambda}^{l'j'\lambda'}(J,B)|^2]\ , \tag{11a}$$

where E is the kinetic energy of the relative motion in the incoming channel, $S_{lj\lambda}^{l'j'\lambda'}(J,A)$ is the S matrix corresponding to the channel states (3a), and the second term in (11a) is the S matrix corresponding to the channel states (3b). It is useful to introduce a collision strength,

$$\Omega(a,b)\equiv\frac{k_a^2}{\pi}(2j_a+1)\sigma(a\to b)\ . \tag{11b}$$

III. APPROXIMATIONS

A. Unitarized Coulomb-Born approximation for large angular momenta

Although one can, in principle, solve Eq. (2b) for all partial waves to obtain the total cross sections, the large number of partial waves contributing to the sum (11a) makes it impractical. Instead, we solve Eq. (2b) for values of J below some critical value $J_{\max}$, and use a more efficient approximation to obtain the partial cross sections from $J_{\max}$ to $J\to\infty$.

At large values of J the scattered projectile can be represented by a Coulomb wave function and at some value, $J=J_{\rm CB}\gg1$, the K matrix obtained from the close-coupled solution approaches $\underline{K}^{\rm CB}$, the K matrix obtained from the Coulomb-Born (CB) approximation. In the unitarized CB approximation, a symmetric K matrix is constructed for the Jth partial wave from the formula[15]

$$\underline{K}_J^{\rm CB}=-\underline{k}^{-1/2}\left[\int_0^\infty dR\,\underline{f}^J(R)2\mu\underline{V}(R)\underline{f}^J(R)\right]\underline{k}^{-1/2}\ , \tag{12}$$

where $\underline{k}$ is a diagonal matrix whose ith element is the wave number of channel i, and $\underline{f}^J(R)$ is a diagonal matrix whose elements $f_{ij}^J(R)$ are the radial Coulomb wave functions regular at the origin. Explicitly,[14]

$$f_{ij}^J(k_iR)=\delta_{ij}\left[e^{-\pi\eta_i/2}\frac{|\,\Gamma(l_i+1+i\eta_i)\,|}{2\Gamma(2l_i+2)}(2k_iR)^{l_i+1}e^{-ik_iR}\,{}_1F_1(l_i+1-i\eta_i,2l_i+2,2ik_iR)\right]\ , \tag{13}$$

where l_i,k_i are, respectively, the projectile angular-momentum quantum number and radial wave number of channel i for the partial wave J. The interaction matrix $\underline{V}(R)$ is the leading term in the asymptotic expansion of expression (8a), as $R\to\infty$. The K matrix then contains elements proportional to the radial integrals,

$$I_{if}^\gamma\equiv\int_0^\infty dR\frac{f_{l_f}(k_fR)f_{l_i}(k_iR)}{R^{\gamma+1}}\ ,$$
$$l_i-l_f\equiv\delta=\gamma,\gamma-2,\ldots,-\gamma\ , \tag{14}$$

where $\gamma=1,2$ for dipole and quadrupole transitions, respectively. These integrals can be expressed in terms of the Appell functions.[16] However, for large $l_i,l_f\gg|\,\eta_i\,|,|\,\eta_f\,|$, and for transitions where the energy defect is small, considerable simplification can be achieved in the evaluation of (14) by replacing the radial functions $f_l(kR)$ by their WKB approximation. Following Alder *et al.*[16] we get

$$I_{ij}^\gamma\approx e^{-{\rm sgn}(q)(\pi/2)|\,\xi\,|}\left[\left[\frac{(Z-1)\mu q}{2\varepsilon\eta^2}\right]^\gamma(|\,2\varepsilon\xi\,|)^{(\gamma-1)/2}\frac{\pi}{2\Gamma\left[\frac{1+\gamma\mp\delta}{2}\right]}W_{\mp\delta/2,-\gamma/2}(|\,2\varepsilon\xi\,|)\right]\ , \tag{15a}$$

where

$$l\equiv(l_i+l_f)/2,\quad \eta\equiv(\eta_i+\eta_f)/2\ ,$$
$$\xi\equiv\eta_f-\eta_i,\quad \varepsilon\equiv\frac{[\eta^2+l(l+1)]^{1/2}}{\eta}\ , \tag{15b}$$

and $W_{\kappa,\mu}(z)$ is the Whittaker function[14] regular at $z\to\infty$. The $\mp$ sign in the expression correspond to the cases when $\varepsilon\xi>0,\varepsilon\xi<0$, respectively. The term in the square brackets is the large l limit of expression (14) when the radial Coulomb functions are replaced by the radial plane-wave functions, the Ricatti-Bessel functions. In the case of dipole transitions ($\gamma=1$), a more accurate approximation to the integral (14) can be obtained which is valid when $\eta\gg1$ regardless of the value of l. It is given by[16]

$$I_{if}^{\gamma=1}\approx-\frac{1}{2}\left[\frac{(Z-1)q\mu}{\eta^2}\right]\xi e^{-(\pi/2)|\xi|}\times\left[\frac{(\varepsilon^2-1)^{1/2}}{\varepsilon}K_{i\xi}(|\varepsilon\xi|)\pm\delta K'_{i\xi}(|\varepsilon\xi|)\right], \tag{16a}$$

where $K_{i\xi}(x)$ is a modified Bessel function,[14]

$$K_\nu(z)=\int_0^\infty e^{-z\cosh(t)}\cosh(\nu t)dt\ , \tag{16b}$$

and $K'_{i\xi}(x)$ is the derivative. When $|\varepsilon\xi|\gg1$, the leading order term in the asymptotic expansion of (15) for the dipole term ($\gamma=1$) and (16a) approach the same limit,

$$\lim_{|\varepsilon\xi|\to\infty}I_{ij}^{\gamma=1}=e^{-(\pi/2)|\xi|}\left[\frac{(Z-1)q\mu}{4\varepsilon\eta^2}\right]\frac{\pi}{\Gamma\left[1\mp\frac{\delta}{2}\right]}\times e^{-|\varepsilon\xi|}(|2\varepsilon\xi|)^{\mp\delta/2}\ . \tag{17}$$

Using (15) and (16) to calculate the K^{CB} matrix when $J\geq J_{CB}$, we obtain the S matrix S^{CB}. This S matrix is unitary for all J since K^{CB} is guaranteed, by construction, to be a symmetric matrix. In Fig. 1 we illustrate the convergence at large J of the close-coupled calculated partial cross sections to the ones obtained in the unitarized Coulomb-Born approximation for the dipole fine-structure transitions in S^{15+} induced by proton impacts.

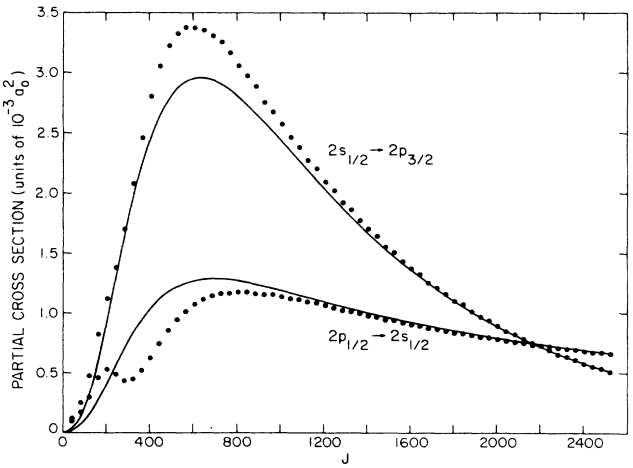

FIG. 1. Comparison between partial cross sections obtained from the close-coupling calculations (dotted line) and the unitarized Coulomb-Born approximation (solid line) for the dipole transitions induced by proton impacts on S^{15+} at a collision energy E of 270 eV.

B. Relativistic effects

For highly charged ions relativistic effects are significant and the scattering formalism must be modified. We may distinguish between two relativistic effects. The first, which we have already implicitly included, consists of the energy splittings of the target states, the $2p_{1/2}$-$2p_{3/2}$ splitting due to the spin-orbit interaction between the bound electron and the nucleus, and the $2s_{1/2}$-$2p_{1/2}$ splitting, the Lamb shift due to the interaction of the electron with virtual photons and positrons. The energy splittings[17] are reproduced in Table II. The second effect is the change in the target-state eigenfunctions.

When the target states of the ion are described by Dirac spinors, the expansion (2a) must be generalized. The scattered projectile is still essentially nonrelativistic, so that we can use Hamiltonian (1), where now $H(r)$ is a single-particle central field Dirac Hamiltonian. The expansion kets $|\Gamma\rangle$ no longer diagonalize the operator $H(\mathbf{r})$, and new channel states $|\Gamma_R\rangle$ are used in the close-coupling expansion (2a). These channel states are linear combinations of the Dirac wave functions $|jm\kappa n\rangle$, where j,m are the total and azimuthal angular-momentum quantum numbers of the electron, κ is the Dirac quantum number which is related to the relativistic parity operator, and n is the principal quantum number. These kets can be represented by the spinor[18]

$$|jm\kappa n\rangle\equiv\frac{1}{r}\begin{bmatrix}P_{j\kappa n}(r) & \chi^m_{j\kappa}(\theta,\phi)\\ iQ_{j\kappa n}(r) & \chi^m_{j-\kappa}(\theta,\phi)\end{bmatrix}, \tag{18}$$

where $\chi^m_{j,\kappa}(\theta,\phi)$ is a two-component spin-orbit function with the properties

$$\mathbf{j}\cdot\mathbf{j}\chi^m_{j\kappa}=j(j+1)\chi^m_{j\kappa}\ ,$$
$$j_z\chi^m_{j\kappa}=m\chi^m_{j\kappa}\ , \tag{19}$$
$$(1+\boldsymbol{\sigma}\cdot\boldsymbol{\lambda})\chi^m_{j\kappa}=-\kappa\chi^m_{j\kappa}\ ,$$

and $\mathbf{j},\boldsymbol{\lambda}$ are, respectively, the total and orbital angular-momentum operators and $\boldsymbol{\sigma}$ is the Pauli spin matrix. For a given value of j the Dirac quantum number κ specifies

TABLE II. Values for the energy splittings (a.u.) of the $n=2$ sublevels used in our calculations. All values are obtained from Ref. 17, except for the values for the ion He^+ which are taken from Ref. 9.

Ion	$\Delta E(2p_{1/2}$-$2s_{1/2})$	$\Delta E(2p_{3/2}$-$2p_{1/2})$
He^+	2.14×10^{-6}	2.66×10^{-5}
C^{5+}	1.19×10^{-4}	2.16×10^{-3}
Mg^{11+}	1.42×10^{-3}	3.48×10^{-2}
S^{15+}	3.92×10^{-3}	0.106
Ar^{17+}	0.006	0.177

the orbital angular-momentum quantum number λ of the spin-orbit functions such that

$$\boldsymbol{\lambda}\cdot\boldsymbol{\lambda}\chi^m_{j\kappa}=\lambda(\lambda+1)\chi^m_{j\kappa}\,,$$
$$\lambda=j+\tfrac{1}{2},\quad \kappa>0 \qquad (20)$$
$$\lambda=j-\tfrac{1}{2},\quad \kappa<0\,.$$

The amplitudes $P_{j\kappa n}, Q_{j\kappa n}$ are, respectively, the "large" and "small" components of the radial wave function. With these target states we can construct channel states $|\Gamma_R\rangle\equiv|JMlj\kappa n\rangle$ where JMl are the same quantum numbers as in the nonrelativistic channel states, and $j\kappa n$ are the relativistic quantum numbers assigned to the bound electron. Using these channel states in the close-coupling expansion (2a), we calculate the potential matrix $\langle\Gamma_R|V|\Gamma'_R\rangle$. The resulting expression is the same as Eq. (5b) except for the replacement of the reduced matrix element

$$\left\langle j\lambda n\left|\left|\frac{r_<^k}{r_>^{k+1}}C_k\right|\right|j'\lambda' n'\right\rangle$$

by

$$\left\langle j\kappa n\left|\left|\frac{r_<^k}{r_>^{k+1}}C_k\right|\right|j'\kappa' n'\right\rangle=\int_0^\infty dr\frac{r_<^k}{r_>^{k+1}}[P_{j\kappa n}(\mathbf{r})P_{j'\kappa' n'}(\mathbf{r})\langle j\kappa||C_k(r)||j'\kappa'\rangle+Q_{j\kappa n}(r)Q_{j'\kappa' n'}(r)\langle j-\kappa||C_k(r)||j'-\kappa'\rangle]\,, \qquad (21)$$

where the ket $|jm\kappa\rangle\equiv\chi^m_{j\kappa}$. Using[12]

$$\langle j\lambda=j\pm\tfrac{1}{2}||C_k(r)||j'\lambda'=j'\pm\tfrac{1}{2}\rangle$$
$$=(-1)^{j+1/2}[j,j']^{1/2}\begin{pmatrix} j & k & j' \\ \frac{1}{2} & 0 & -\frac{1}{2}\end{pmatrix},$$
$$\lambda+\lambda'+k=0,2,\ldots \qquad (22)$$

and Eq. (20) we get

$$\langle j\kappa||C_k(r)||j'\kappa'\rangle=\langle j-\kappa||C_k(r)||j'-\kappa'\rangle$$
$$=(-1)^{j+1/2}[j,j']^{1/2}\begin{pmatrix} j & k & j' \\ \frac{1}{2} & 0 & -\frac{1}{2}\end{pmatrix} \qquad (23)$$

provided that $\lambda+\lambda'+k$ is an even integer. We then obtain

$$\langle\Gamma_R|V|\Gamma'_R\rangle=q\left[\delta_{\Gamma,\Gamma'}\left(\frac{Z}{R}-R^{j\kappa n}_{j\kappa n}(0,R)\right)-\delta_{J,J'}\delta_{M,M'}V^{lj\kappa n}_{l'j'\kappa' n'}(J,R)\right], \qquad (24a)$$

where

$$V^{lj\kappa n}_{l'j'\kappa' n'}(J,R)=\sum_{k=1}^{\infty}Q^{lj\kappa}_{l'j'\kappa'}(k,J)R^{j\kappa n}_{j'\kappa' n'}(k,R) \qquad (24b)$$

and $Q^{lj\kappa}_{l'j'\kappa'}$ is identical to the expression on the right-hand side of Eq. (8c). The new radial potentials $R^{j\kappa n}_{j'\kappa' n'}$ are obtained by replacing the functions $P_{n\lambda}(r)P_{n'\lambda'}(r)$ in Eq. (7) by

$$P_{j\kappa n}(r)P_{j'\kappa' n'}(r)+Q_{j\kappa n}(r)Q_{j'\kappa' n'}(r)\,. \qquad (25)$$

For the radial wave functions we use the Dirac-Coulomb radial functions given in Rose.[18] Unlike the nonrelativistic integral this integral cannot be expressed in terms of elementary functions. In the case of proton-impact excitation we can adequately approximate the radial potential by

$$R^{j\kappa n}_{j'\kappa' n'}(k,R)\approx\frac{1}{R^{k+1}}\int_0^\infty dr[P_{nj\kappa}(r)P_{n'j'\kappa'}(r)+Q_{nj\kappa}(r)Q_{n'j'\kappa'}(r)] \qquad (26)$$

provided that the collision energy is such that the distance of closest approach, $(Z-1)/E$, is greater than the size of the ion. This integral may be evaluated in a straightforward manner but it is more useful to express (26) as an expansion in powers of $Z\alpha$ where $\alpha\approx\frac{1}{137}$ is the fine-structure constant. To an accuracy up to order $(Z\alpha)^2$,

$$ZR^{1/2\,12}_{1/2-12}(k=1,R)=\frac{-3\sqrt{3}}{R^2}[1-\tfrac{5}{12}(Z\alpha)^2]\,,$$
$$ZR^{1/2-12}_{3/2-22}(k=1,R)=\frac{-3\sqrt{3}}{R^2}[1-\tfrac{1}{6}(Z\alpha)^2]\,, \qquad (27)$$
$$Z^2R^{1/2\,12}_{3/2-22}(k=2,R)=\frac{30}{R^3}[1-\tfrac{21}{40}(Z\alpha)^2]\,,$$

where we have used the quantum-number assignments: $n=n'=2$, $j=\frac{1}{2}$, and $\kappa=-1$ for the $s_{1/2}$ state; $j=\frac{1}{2}$ and $\kappa=1$ for the $p_{1/2}$ state; and $j=\frac{3}{2}$ and $\kappa=-2$ for the $p_{3/2}$ state. In the collisional excitation of the $n=2$ levels in Ar^{17+} we found that the relativistic correction is about one percent of the nonrelativistic cross section. Relativistic corrections are expected to become significant for hydrogenlike ions only when $Z>30$.

C. Plasma-density effects

In a sufficiently dense plasma the independent-particle collisional model is inadequate. The interactions of the plasma constituents, the electrons and protons, with impurity ions can no longer be described by the direct long-range Coulomb interaction of the projectile with the target. However, for many plasma environments, many-body effects can be represented approximately by a

single-particle projectile-ion potential provided that the long-range Coulomb interaction is sufficiently screened. Two of the most common screening models are the Debye-Hückel (DH) model which adequately describes the electrostatic interaction between the constituents of a dense plasma in the high-temperature limit and the ion-sphere model appropriate in the low-temperature limit. A critical discussion of the validity of the various models is given by Weisheit.[10] Whitten *et al.*[11] investigated the electron-impact excitation of the $n=1,2$ levels in hydrogenlike ions using both the DH model and the ion-sphere model, and Scheiber *et al.*[19] investigated proton-impact excitation of the $n=2$ fine-structure transitions using a semiclassical scattering formalism. We will present the results of a close-coupling calculation for the excitation of the $n=2$ levels in Ar^{17+} by electrons and protons, when the projectile-ion interaction is described by a Debye-Hückel potential, and the influence of the plasma environment on the level shifts of the ion is neglected.[11]

Following Whitten *et al.*,[11] we model the electron-ion interaction by the potential

$$V_{\mathrm{DH}}(\mathbf{R},\mathbf{r})=\left[\frac{-Z}{R}+\frac{1}{|\mathbf{R}-\mathbf{r}|}\right]\exp(-R/\Lambda)\ , \tag{28}$$

where Λ is the Debye length,

$$\Lambda=\left[\frac{kT}{4\pi e^2 n_e}\right]^{1/2}\ , \tag{29}$$

n_e is the electron density in the plasma, and T is the electron temperature. We model the proton-ion interaction by (28) with the term in brackets multiplied by an overall minus sign. Using the projectile-ion potential (28), the scattering formalism is identical to that given earlier, except for the multiplication of the radial matrix elements (7) by an overall screening factor, $\exp(-R/\Lambda)$, and the replacement of the asymptotic Coulomb wave functions in (10a) by the corresponding Ricatti-Bessel functions.

IV. RESULTS AND DISCUSSION

The calculated cross sections for proton-impact excitation of the $n=2$ fine-structure levels of the hydrogenlike ions Ar^{17+}, S^{15+}, Mg^{11+}, C^{5+}, and He^{+} are presented in Table III and in Figs. 2(a)–2(c). In Figs. 2 the cross sections, scaled by a factor Z^4, Z being the nuclear charge of the ion, are tabulated as a function of the relative collision energy expressed in terms of electron volts scaled by a factor of Z^{-2}.

The proton-impact-excitation cross sections are negligible at low relative collision velocities of the proton-ion system, and remain very small at velocities far above the transition excitation threshold. In the Coulomb-Born approximation the dipole cross sections behave as[16]

$$\sigma\propto\frac{1}{E}\exp(-2\pi|\xi|) \tag{30}$$

in the region where they are initially rising with increasing collision velocity. The parameter ξ is given by (15b), and can be expressed at small transition energies $\Delta\varepsilon$ such that $\Delta\varepsilon/E\ll 1$, as

$$\xi\approx(Z-1)\frac{\Delta\varepsilon}{2vE}=\Delta\varepsilon\Big/\left[\frac{v}{R_c}\right],\quad R_c\equiv\frac{(Z-1)}{2E} \tag{31}$$

where v is the relative collision velocity. The dimensionless parameter ξ is the ratio of the time for the proton to travel one-half the distance of closest approach in a head-

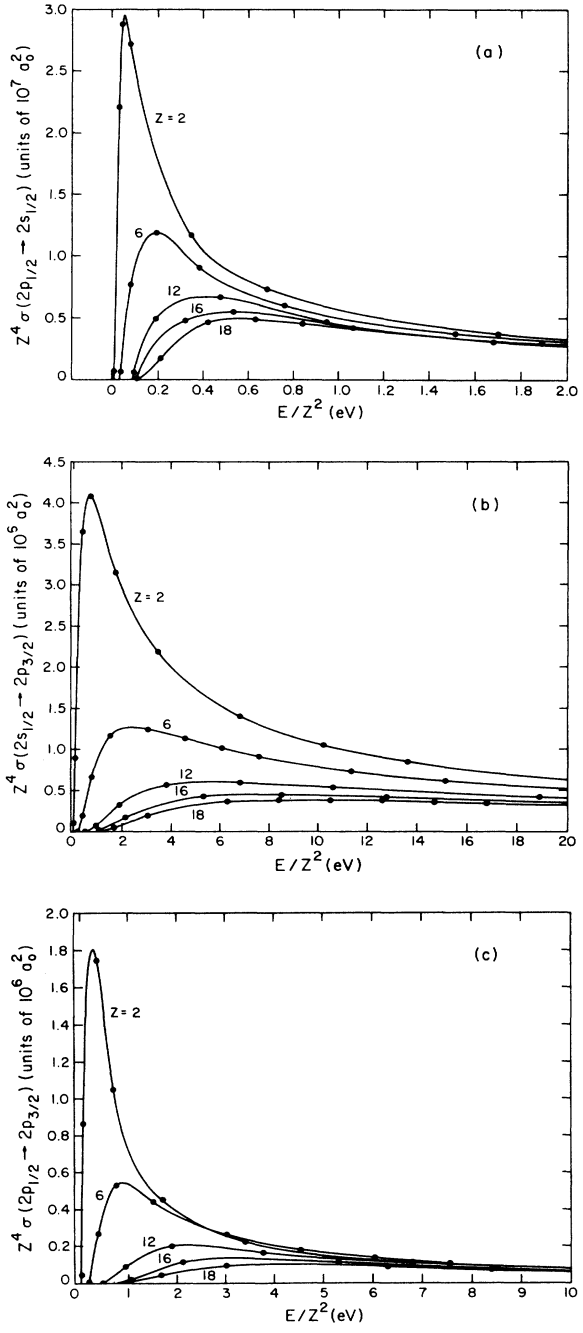

FIG. 2. Proton-impact-excitation cross sections for the ions Ar^{17+}, S^{15+}, Mg^{11+}, C^{5+}, and He^{+}: (a) the $2p_{1/2}$-$2s_{1/2}$ transition, (b) the $2s_{1/2}$-$2p_{3/2}$, (c) the $2p_{1/2}$-$2p_{3/2}$ transition. The solid lines are spline fits to the calculated values (circles) listed in Table III. The cross sections are scaled by a factor Z^4 and are expressed as a function of the scaled collision energy EZ^{-2} (eV).

TABLE III. Proton-impact-excitation cross sections for the $n=2$ levels in the ions Ar^{17+}, S^{15+}, Mg^{11+}, C^{5+}, and He^{+}. The cross sections are expressed in units of a_0^2, as a function of the scaled energy $E_T(\mathrm{eV})Z^{-2}$. The energy E_T is measured with respect to the $2p_{1/2}$ level.

$E_T(\mathrm{eV})Z^{-2}$	$\sigma(2p_{1/2}\rightarrow 2s_{1/2})$	$\sigma(2s_{1/2}\rightarrow 2p_{3/2})$	$\sigma(2p_{1/2}\rightarrow 2p_{3/2})$
		Ar^{17+}	
0.084	0.028		
0.21	16.4		
0.42	44.2		
0.63	46.6	1.0×10^{-4}	6.5×10^{-5}
0.84	43.4	5.8×10^{-3}	5.1×10^{-3}
1.68	29.5	0.46	0.437
3.02	19.5	1.86	0.946
6.30	11.2	3.50	0.871
8.40	9.01	3.65	0.687
10.50	7.57	3.66	0.582
12.60	6.51	3.64	0.495
14.70	5.79	3.45	0.440
16.80	5.20	3.31	0.392
20.16	4.48	3.10	0.329
25.19	3.74	2.78	0.257
33.59	2.94	2.54	0.181
		S^{15+}	
0.106	2.17		
0.319	72.7		
0.531	84.0	2.81×10^{-4}	1.89×10^{-4}
1.063	64.5	0.292	0.326
2.126	40.6	2.61	1.78
5.314	20.8	6.51	1.78
8.503	14.4	6.80	1.20
12.75	10.5	6.41	0.851
17.01	8.30	5.79	0.661
21.26	6.93	5.33	0.521
25.51	5.98	4.82	0.433
38.26	4.27	3.81	0.265
		Mg^{11+}	
0.094	30.6		
0.189	2.39×10^{2}		
0.472	3.22×10^{2}	0.06	0.06
0.945	2.28×10^{2}	3.60	4.32
1.890	1.44×10^{2}	15.6	9.69
3.780	86.6	27.1	8.02
6.803	55.4	28.7	5.29
10.58	39.2	26.0	3.66
18.90	24.6	20.2	2.07
23.62	20.5	17.7	1.60
24.56	19.8	17.4	1.54
27.21	18.3	16.4	1.38
		C^{5+}	
0.0378	5.17×10^{2}		
0.0756	5.93×10^{3}		
0.189	9.17×10^{3}	7.40	6.26
0.378	7.01×10^{3}	1.53×10^{2}	2.07×10^{2}
0.756	4.64×10^{3}	5.18×10^{2}	4.10×10^{2}
1.512	2.91×10^{3}	8.99×10^{2}	3.40×10^{2}
3.023	1.76×10^{3}	9.61×10^{2}	2.04×10^{2}
4.535	1.29×10^{3}	8.75×10^{2}	1.40×10^{2}
6.047	1.03×10^{3}	7.83×10^{2}	1.07×10^{2}
11.34	6.24×10^{2}	5.71×10^{2}	5.73×10^{1}
15.12	4.93×10^{2}	4.79×10^{2}	4.30×10^{1}
24.19	3.24×10^{2}	3.51×10^{2}	2.57×10^{1}
34.01	2.51×10^{2}	2.79×10^{2}	1.86×10^{1}

TABLE III. (*Continued*).

$E_T(\text{eV})Z^{-2}$	$\sigma(2p_{1/2}\rightarrow 2s_{1/2})$	$\sigma(2s_{1/2}\rightarrow 2p_{3/2})$	$\sigma(2p_{1/2}\rightarrow 2p_{3/2})$
		He^+	
0.0068	4.67×10^{4}	0.12	
0.0204	1.38×10^{6}	1.02×10^{2}	15.2
0.034	1.80×10^{6}	6.95×10^{3}	2.91×10^{3}
0.068	1.70×10^{6}	5.59×10^{4}	5.41×10^{4}
0.340	7.30×10^{5}	2.28×10^{5}	1.09×10^{5}
0.680	4.58×10^{5}	2.55×10^{5}	6.55×10^{4}
1.701	2.34×10^{5}	1.97×10^{5}	2.82×10^{4}
3.40	1.36×10^{5}	1.37×10^{5}	1.41×10^{4}
6.80	7.76×10^{4}	8.77×10^{4}	7.20×10^{3}
10.20	5.56×10^{4}	6.59×10^{4}	4.82×10^{3}
13.61	4.34×10^{4}	5.32×10^{4}	3.64×10^{3}
23.81	2.72×10^{4}	3.50×10^{4}	2.03×10^{3}
34.01	1.98×10^{4}	2.66×10^{4}	1.42×10^{3}

on collision to the time scale of the induced atomic transition. Thus the vanishing of the cross sections is a consequence of the transition becoming adiabatic at small collision velocities.[20] At large collision energies the Coulomb-Born approximation predicts the excitation cross sections to behave as

$$\sigma \propto \frac{1}{E}\ln\left[\frac{1.12(1-\pi\xi)}{\xi}\right] . \tag{32}$$

Using (32) we solve for ξ_0, the value of the ξ parameter where the cross section passes through a maximum. Differentiating (32) with respect to E and setting the resulting expression to zero, we obtain the transcendental equation for ξ_0,

$$\xi_0 = 1.12\exp\left[\frac{-3}{2(1-\pi\xi_0)}\right] , \tag{33}$$

whose solution is $\xi_0 \approx 0.112$. Using (31), the value of ξ_0, and the level splittings given in Table II, we calculate $E^{\max}$, the value of the collision energy where the $2p_{1/2}$-$2s_{1/2}$ cross sections are at a maximum. The results for $E^{\max}/Z^2$ are 0.48 eV for Ar^{17+}, 0.31 eV for Mg^{11+}, 0.14 eV for C^{5+}, and 0.03 eV for He^+. These values for $E^{\max}$ are consistent with the cross sections illustrated in Fig. 2(a). Although the Coulomb-Born approximation predicts successfully the approximate location of $E^{\max}$, it gives poor results for the absolute value of the cross sections, primarily because of the violation of unitarity. In Fig. 3 the cross sections calculated using the Coulomb-Born approximation for the dipole transitions induced by proton impacts on Ar^{17+} are compared with the close-coupled results. Despite the deficiencies of the Coulomb-Born approximation, it does explain, qualitatively, the sensitivity of the dipole-induced cross sections to the value of ξ. The value of ξ is very different for the two transitions at a given collision energy because of the disparity in the transition energy defects, the $2p_{1/2}$-$2s_{1/2}$ being 10 to 30 times smaller than the $2s_{1/2}$-$2p_{3/2}$ energy defect for the ions under consideration. Thus, when the $2p_{1/2}$-$2s_{1/2}$ cross section is at a maximum, the $2s_{1/2}$-$2p_{3/2}$ transition is still adiabatic, the cross section becoming appreciable only at an energy $E \approx E_1^{\max}(\Delta\varepsilon_2/\Delta\varepsilon_1)$, where the subscripts 1 and 2 refer to the $2p_{1/2}$-$2s_{1/2}$ and $2s_{1/2}$-$2p_{3/2}$ transitions, respectively. The ratio of the maxima is given by

$$\frac{\sigma(2p_{1/2}\rightarrow 2s_{1/2})_{\max}}{\sigma(2s_{1/2}\rightarrow 2p_{3/2})_{\max}} = \frac{1}{2}\frac{E_1^{\max}}{E_2^{\max}} , \tag{34}$$

where we have used (32) and included the statistical factor of $\frac{1}{2}$. With the values of $E_1^{\max}$ and $E_2^{\max}$ obtained from the close-coupling calculations, expression (34) roughly predicts the correct ratios, ≈ 10, over the range of ions we have considered.

In Figs. 4(a)—4(c) we present the results for the electron-impact-excitation collision strengths of the $n=2$ fine-structure levels. The electron-impact cross sections differ from the proton-impact cross sections in being finite at the transition energy thresholds.

In the limit of high collision energies, an adequate description of the electron-impact-excitation cross section can be obtained from a Born-approximation treatment and the use of multipole potentials that are sufficiently

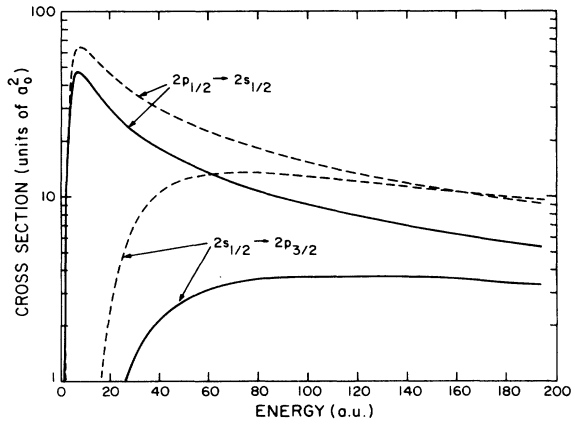

FIG. 3. Comparison between the Coulomb-Born approximation (dashed line) and close-coupling approximation (solid line) for dipole transitions induced by proton impacts on Ar^{17+}.

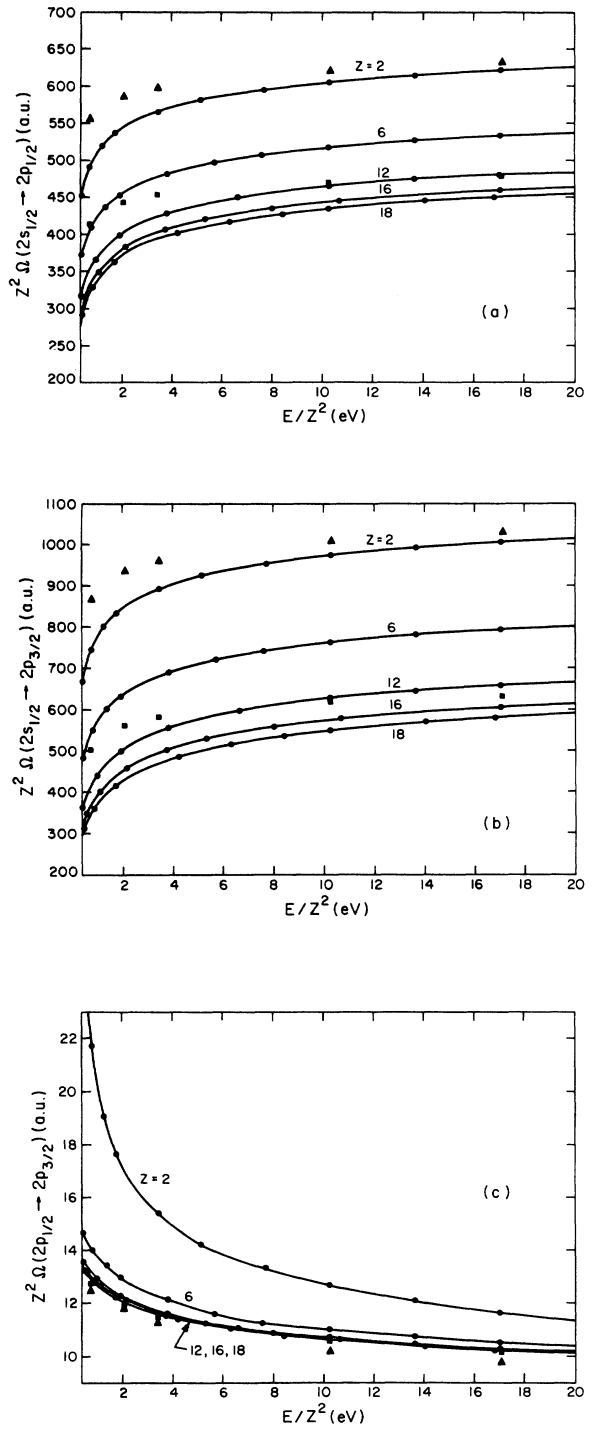

FIG. 4. Electron-impact-excitation collision strengths for the ions Ar^{17+}, S^{15+}, Mg^{11+}, C^{5+}, and He^{+}: (a) the $2p_{1/2}$-$2s_{1/2}$ transition, (b) the $2s_{1/2}$-$2p_{3/2}$ transition, (c) the $2p_{1/2}$-$2p_{3/2}$ transition. The solid lines are spline fits to the calculated values (circles). Collision strengths calculated by Burgess *et al.* (Ref. 6) for electron impacts on He^{+} (triangles) and in the $Z=\infty$ approximation (squares) are included. The collision strengths are scaled by a factor Z^2 and are expressed as a function of the scaled collision energy EZ^{-2}.

screened for close electron-ion encounters.[4] This treatment predicts an asymptotic behavior at high collision energies for the dipole-transition collision strengths,

$$\Omega \propto \ln\left[\frac{1}{\Delta\varepsilon}\frac{v}{R_0}\right], \tag{35}$$

where v is the electron collision velocity and R_0 is an interaction radius of the order of the size of the ion. For

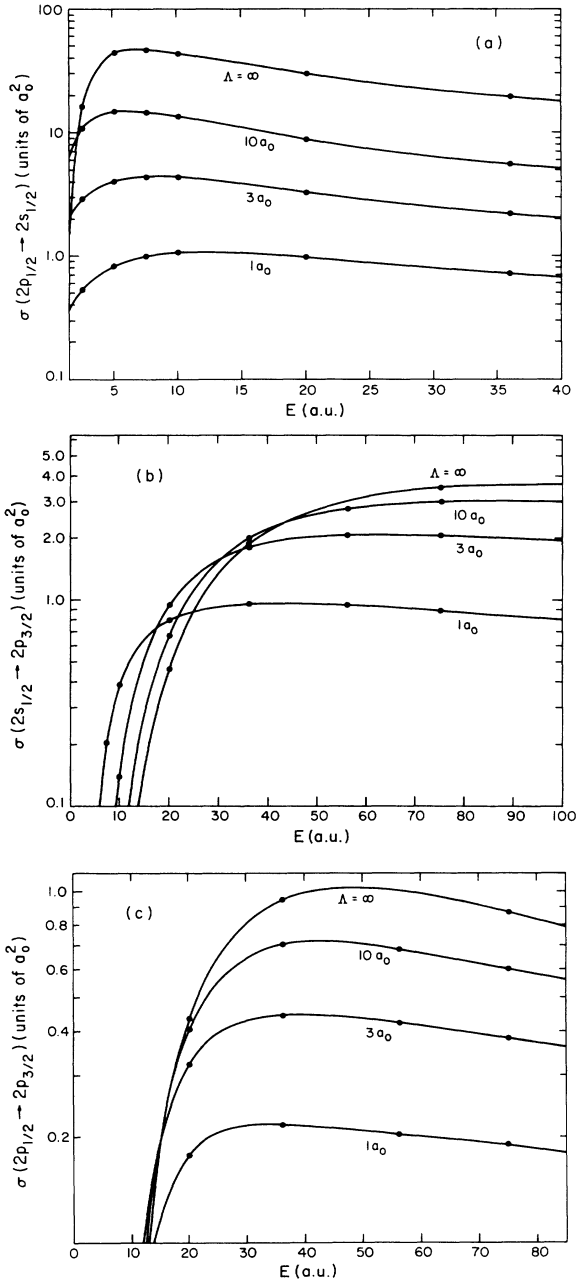

FIG. 5. Proton-impact-excitation cross sections for Ar^{17+} for various values of the Debye length $\Lambda(a_0)$: (a) the $2p_{1/2}$-$2s_{1/2}$ transition, (b) the $2s_{1/2}$-$2p_{3/2}$ transition, (c) the $2p_{1/2}$-$2p_{3/2}$ transition.

the electron collision velocities of interest in this paper the collision time R_0/v is on the order of, or less than, the atomic period $1/\Delta\varepsilon$ and the collision strengths (35) are sensitive to the energy defects of the transitions. The dipole electron-impact-excitation collision strengths become statistical at high collision velocities when $v/R_0 \gg \Delta\varepsilon$.

In Figs. 4(a)—4(c) we reproduce the unitarized Coulomb-Born-approximation calculations of Burgess *et al.*[9] for electron-impact-excitation collision strengths and compare them to our close-coupling values. The Coulomb-Born results for the dipole excitation $2p_{1/2}$-$2s_{1/2}$ and $2s_{1/2}$-$2p_{3/2}$ collision strengths are consistent with our values for the excitation of He^+, and for the excitation of Ar^{17+} the $Z=\infty$ calculation of Burgess *et al.* is also in agreement with our values. For the quadrupole transition, there is close agreement between the $Z=\infty$ calculation of Burgess *et al.* and our results for the $2p_{1/2}$-$2p_{3/2}$ excitation in Ar^{17+}. For He^+ the agreement is less satisfactory, especially near the transition threshold where close-coupling effects are significant. However, exchange effects are also important near threshold. More accurate calculations are needed.

The high-energy, asymptotic, electron-impact-excitation collision strengths may be obtained by a least-square fit of the calculated close-coupling results to the functional form,

$$\Omega = c_1 \ln(E) + c_2 + \frac{c_3}{E} + \frac{c_4}{E^2} . \tag{36}$$

An analogous fit may be performed for the proton-impact-excitation cross sections. For the quadrupole transitions the coefficients c_1 are zero. Using the calculated

TABLE IV. Proton-impact-excitation rate coefficients for the $n=2$ levels in the ions Ar^{17+}, S^{15+}, Mg^{11+}, C^{5+}, and He^+. The Z^3 scaled rates are expressed in units of 10^{-7} cm^3 sec^{-1}, as a function of the scaled temperature $\theta \equiv kTZ^{-2}$ (a.u.).

θ	$Z^3C(2p_{1/2}\rightarrow 2s_{1/2})$	$Z^3C(2s_{1/2}\rightarrow 2p_{3/2})$	$Z^3C(2p_{1/2}\rightarrow 2p_{3/2})$
		Ar^{17+}	
0.025	1.27×10^{3}	1.70×10^{1}	1.08×10^{1}
0.05	1.38×10^{3}	7.35×10^{1}	3.21×10^{1}
0.10	1.31×10^{3}	1.87×10^{2}	5.54×10^{1}
0.20	1.17×10^{3}	3.28×10^{2}	6.68×10^{1}
0.40	9.90×10^{2}	4.48×10^{2}	6.39×10^{1}
0.80	8.16×10^{2}	5.19×10^{2}	5.25×10^{1}
		S^{15+}	
0.025	1.38×10^{3}	2.85×10^{1}	1.80×10^{1}
0.05	1.45×10^{3}	1.04×10^{2}	4.59×10^{1}
0.10	1.35×10^{3}	2.36×10^{2}	7.08×10^{1}
0.20	1.19×10^{3}	3.86×10^{2}	7.90×10^{1}
0.40	1.01×10^{3}	5.00×10^{2}	7.22×10^{1}
0.80	8.28×10^{2}	5.53×10^{2}	5.79×10^{1}
		Mg^{11+}	
0.025	1.55×10^{3}	6.62×10^{1}	4.06×10^{1}
0.05	1.55×10^{3}	1.85×10^{2}	7.59×10^{1}
0.10	1.42×10^{3}	3.53×10^{2}	9.76×10^{1}
0.20	1.23×10^{3}	5.12×10^{2}	9.90×10^{1}
0.40	1.04×10^{3}	6.12×10^{2}	8.58×10^{1}
0.80	8.51×10^{2}	6.39×10^{2}	6.72×10^{1}
		C^{5+}	
0.025	1.95×10^{3}	3.20×10^{2}	1.46×10^{2}
0.05	1.81×10^{3}	5.57×10^{2}	1.71×10^{2}
0.10	1.59×10^{3}	7.64×10^{2}	1.62×10^{2}
0.20	1.35×10^{3}	8.85×10^{2}	1.35×10^{2}
0.40	1.12×10^{3}	9.12×10^{2}	1.04×10^{2}
0.80	9.08×10^{2}	8.67×10^{2}	7.67×10^{1}
		He^+	
0.025	2.54×10^{3}	1.35×10^{3}	3.16×10^{2}
0.05	2.21×10^{3}	1.57×10^{3}	2.65×10^{2}
0.10	1.86×10^{3}	1.62×10^{3}	2.06×10^{2}
0.20	1.52×10^{3}	1.54×10^{3}	1.55×10^{2}
0.40	1.22×10^{3}	1.37×10^{3}	1.14×10^{2}
0.80	9.62×10^{2}	1.19×10^{3}	8.20×10^{1}

cross sections for the fine-structure transitions by protons and electrons, we obtain the excitation rate coefficient for a transition from state i to state j as an average of the product of the cross sections and the projectile velocity over a Maxwellian distribution of the impact velocities at temperature T,

$$C(i\rightarrow j)=\left[\frac{8kT}{\mu\pi}\right]^{1/2}\left[\frac{1}{kT}\right]^{2} \times\int_{\Delta\varepsilon}^{\infty}E\sigma_{ij}(E)\exp\left[-\frac{E}{kT}\right]dE\ . \quad (37)$$

These rate coefficients are listed in Tables IV and V. Deexcitation rate coefficients can be obtained using the principle of detailed balance. In Table VI we compare our rate coefficients for the $2p_{1/2}$-$2s_{1/2}$ and $2s_{1/2}$-$2p_{3/2}$ transitions by proton impacts on Mg^{11+} and S^{15+} with the semiclassical calculations of Beigman *et al.*[5] The $2s_{1/2}$-$2p_{1/2}$ excitation rate coefficients for Mg^{11+} calculated by Beigman *et al.* are about 20% larger than our rate-coefficients transition at a temperature kT of 98 eV and the semiclassical $2s_{1/2}$-$2p_{3/2}$ rate coefficient is about twice as large as our rate coefficient. At higher temperatures, the semiclassical rate coefficients and close-coupling-calculation rate coefficients seem to converge.

In Figs. 5(a)—5(c) we present the close-coupling results for the proton-impact excitation of the $n=2$ fine-structure levels in Ar^{17+} with the proton-ion interaction given by the Debye-Hückel potential (28) with Debye lengths $\Lambda=1a_0$, $3a_0$, and $10a_0$. The cross sections for the long range $\Lambda=\infty$ case are included for comparison.

TABLE V. Electron-impact-excitation rate coefficients for the $n=2$ levels in the ions Ar^{17+}, S^{15+}, Mg^{11+}, C^{5+}, and He^{+}. The Z^3 scaled rates are expressed in units of 10^{-7} cm^3 sec^{-1}, as a function of the scaled temperature $\theta\equiv kTZ^{-2}$ (a.u.).

θ	$Z^3C(2p_{1/2}\rightarrow 2s_{1/2})$	$Z^3C(2s_{1/2}\rightarrow 2p_{3/2})$	$Z^3C(2p_{1/2}\rightarrow 2p_{3/2})$
		Ar^{17+}	
0.025	1.36×10^{2}	1.50×10^{2}	5.94
0.05	1.09×10^{2}	1.23×10^{2}	4.20
0.10	8.55×10^{1}	9.95×10^{1}	2.90
0.20	6.58×10^{1}	7.90×10^{1}	1.98
0.40	4.98×10^{1}	6.17×10^{1}	1.34
0.80	3.72×10^{1}	4.76×10^{1}	9.10×10^{-1}
		S^{15+}	
0.025	1.38×10^{2}	1.57×10^{2}	5.89
0.05	1.11×10^{2}	1.30×10^{2}	4.19
0.10	8.74×10^{1}	1.05×10^{2}	2.91
0.20	6.72×10^{1}	8.30×10^{1}	1.98
0.40	5.09×10^{1}	6.48×10^{1}	1.35
0.80	3.81×10^{1}	4.97×10^{1}	9.13×10^{1}
		Mg^{11+}	
0.025	1.43×10^{2}	1.70×10^{2}	5.60
0.05	1.17×10^{2}	1.42×10^{2}	4.10
0.10	9.20×10^{1}	1.15×10^{2}	2.88
0.20	7.07×10^{1}	9.12×10^{1}	1.98
0.40	5.34×10^{1}	7.07×10^{1}	1.35
0.80	3.98×10^{1}	5.41×10^{1}	9.14×10^{-1}
		C^{5+}	
0.025	1.78×10^{2}	2.35×10^{2}	6.82
0.05	1.39×10^{2}	1.88×10^{2}	4.67
0.10	1.06×10^{2}	1.48×10^{2}	3.16
0.20	8.02×10^{1}	1.14×10^{2}	2.11
0.40	5.99×10^{1}	8.69×10^{1}	1.41
0.80	4.42×10^{1}	6.52×10^{1}	9.46×10^{-1}
		He^{+}	
0.025	1.87×10^{2}	2.84×10^{2}	8.32
0.05	1.56×10^{2}	2.40×10^{2}	6.02
0.10	1.23×10^{2}	1.91×10^{2}	4.06
0.20	9.36×10^{1}	1.48×10^{2}	2.64
0.40	7.01×10^{1}	1.12×10^{2}	1.70
0.80	5.19×10^{1}	8.36×10^{1}	1.09

TABLE VI. Comparison between the close-coupling (CC) approximation rate coefficients, and the ones obtained by the semiclassical calculations (SC) of Beigman *et al.* (Ref. 5) for the dipole transitions induced by proton impacts on the ions Mg^{11+} and S^{15+}. All rates are expressed in units of 10^{-9} cm^3 sec^{-1}.

kTZ^{-2} (eV)	$C(2p_{1/2}\rightarrow 2s_{1/2})$		$C(2s_{1/2}\rightarrow 2p_{3/2})$	
		Mg^{11+}		
	CC	SC	CC	SC
0.68	89.9	111	3.83	7.59
1.36	89.8	107	10.7	16.2
2.04	83.8	99.2	16.3	22.2
2.72	82.2	93.7	20.4	25.7
5.44	71.4	78.4	29.7	34.3
		S^{15+}		
	CC	SC	CC	SC
0.68	33.8	39.4	0.69	1.47
1.36	35.3	40.6	2.53	4.05
2.04	34.3	38.8	4.29	5.88
2.72	33.1	37.0	5.76	7.60

The results illustrate the extreme sensitivity of the cross sections to the value of the Debye screening length. The cross section for the $2p_{1/2}$-$2s_{1/2}$ transition is about 40 times larger, at its peak, for the unscreened $\Lambda=\infty$ case then for $\Lambda=1a_0$. The $2s_{1/2}$-$2p_{3/2}$ cross section is much less sensitive to the value of Λ, the $\Lambda=\infty$ cross section being only about five times as large as the cross section when $\Lambda=1a_0$. Because the $2p_{1/2}$-$2s_{1/2}$ energy defect is much less than the $2s_{1/2}$-$2p_{3/2}$ energy defect, the latter cross sections have more contributions from large partial waves than the former. With Debye screening, the contributions to the cross section coming from partial waves with large angular momenta are diminished and the dipole transitions with smaller energy defects are then more sensitive to the value of the screening parameter. In Figs. 6(a)—6(c) we present the collision strengths for the electron-impact excitation of the $n=2$ fine-structure levels in Ar^{17+} for the same values of Λ. As in the case of proton-ion collisions, the Debye screening of the ion strongly suppresses the dipole-transition cross sections. Unlike the proton-ion dipole cross sections, the $2s_{1/2}$-$2p_{1/2}$ and $2s_{1/2}$-$2p_{3/2}$ electron-impact-transition cross sections have a similar dependence on the Λ parameter, both being about 20 times as large for $\Lambda=\infty$ than for $\Lambda=1a_0$. The quadrupole $2p_{1/2}$-$2p_{3/2}$ transition cross sections are also sensitive to the value of the Debye screening parameter. The cross section corresponding to $\Lambda=\infty$ is about five times larger than the $\Lambda=1a_0$ cross section for proton impacts, and about two times larger for electron impacts. As the value of the Debye parameter is decreased, or the screening is increased, the dipole-transition cross sections approach their statistical ratios at lower values of the collision velocity. This is true for both the proton- and electron-ion collision cross sections and is a consequence of the quenching of the contributions to the cross section coming from large values of the total angular momentum.

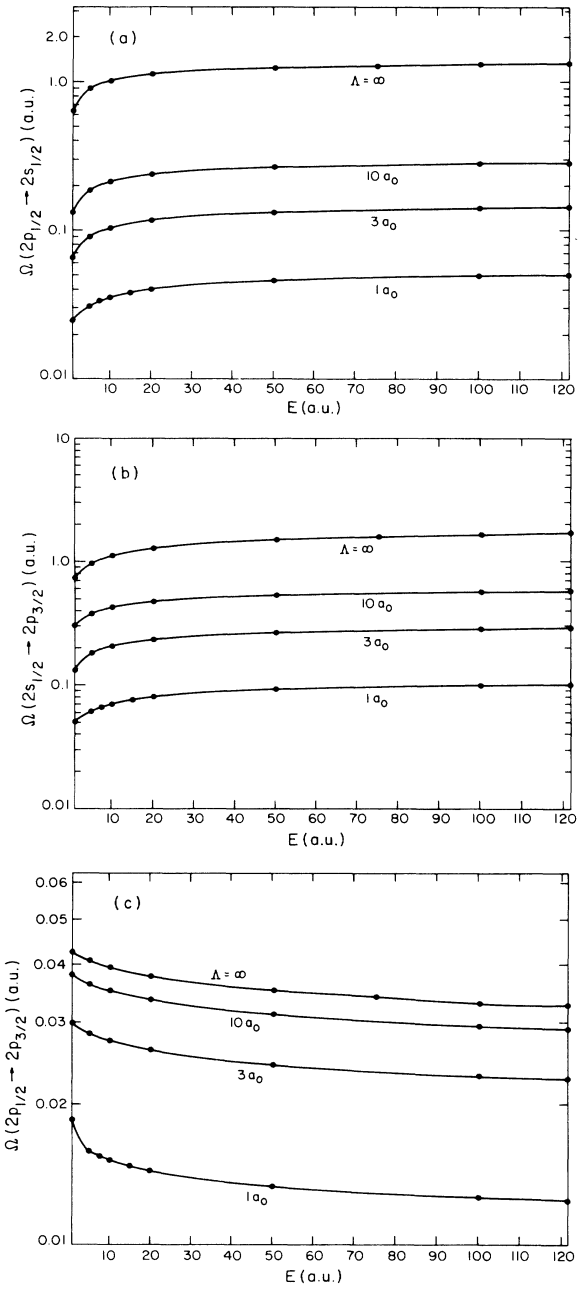

FIG. 6. Electron-impact-excitation collision strengths for Ar^{17+} for various values of the Debye length $\Lambda(a_0)$: (a) the $2p_{1/2}$-$2s_{1/2}$ transition, (b) the $2s_{1/2}$-$2p_{3/2}$ transition, (c) the $2p_{1/2}$-$2p_{3/2}$ transition.

V. THE β RATIO

We consider a plasma composed of a nearly equal number of electrons and protons with Maxwellian velocity distributions characterized by a common temperature T. The plasma contains a small fraction of impurity ions whose level populations N_i are determined by electron- and proton-induced transitions and by radiative transitions. In the steady state

$$N_i \left[A_i + \sum_j \eta C_{ij} \right] = q_i + \sum_j N_j \eta C_{ji} \ , \tag{38}$$

where A_i is the radiative decay rate out of level i, η is the electron and proton number density, C_{ij} is the sum of the rate coefficients for electron- and proton-impact excitation of the transition from level i to level j, and q_i is the rate at which level i is populated from states external to the set included in the summations. We restrict the summations to the fine-structure levels of the $n=2$ state of an impurity hydrogenlike heavy ion. The spontaneous decay rates A_i are the sum of the $2s_{1/2}$-$1s_{1/2}$ two photon electric dipole rate and the single-photon magnetic dipole rate[21] and the $2p_{1/2,3/2}$-$1s_{1/2}$ single-photon electric dipole rates. The rate coefficients C_{ij} are those presented in Tables IV and V. For q_i we adopt rates correpsonding to electron-impact excitation from the $1s$ level.[22] A more comprehensive study for Mg^{11+} has been carried out by

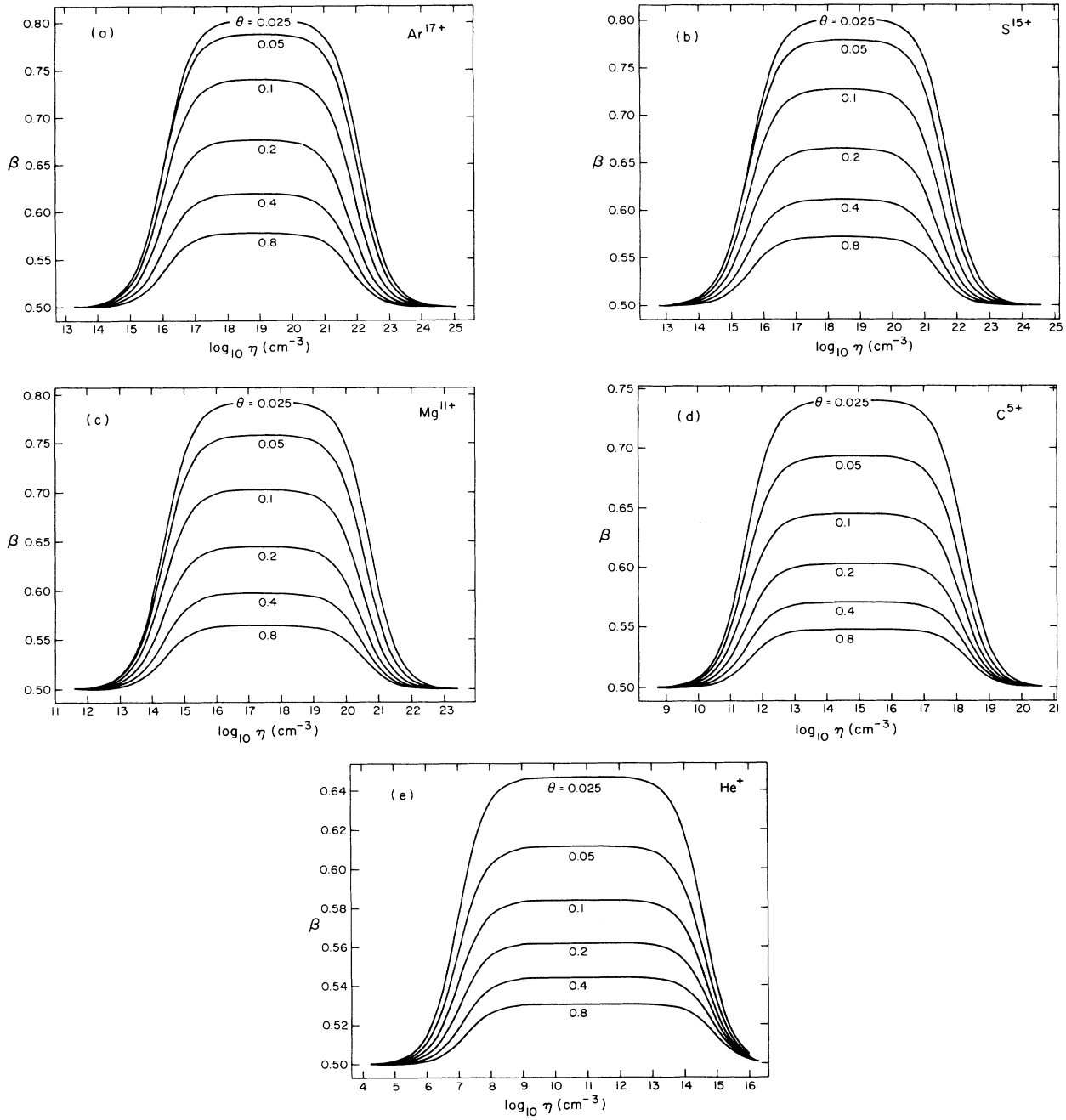

FIG. 7. The β parameter as a function of the electron density for the ions (a) Ar^{17+}, (b) S^{15+}, (c) Mg^{11+}, (d) C^{5+}, (e) He^+. The temperature of the plasma corresponds to the values of $\theta \equiv kTZ^{-2}$ (a.u.) of 0.025, 0.05, 0.1, 0.2, 0.4, and 0.8.

Ljepojevic *et al.*[6] in which levels up to large principle quantum numbers were included. The values of β differ from those attained in the four-state model by about 5%.

In Fig. 7 we present the calculated β ratios as functions of the electron density for various values of the temperature T of the ions He^+, C^{5+}, Mg^{11+}, S^{15+}, and Ar^{17+}. As shown by Beigman *et al.*,[5] Vinogradov *et al.*,[4] and Ljepojevic *et al.*,[6] the ratio departs from the statistical value for a range of densities at which the collision-induced transition rates lie between the radiative decay rate of the $2s_{1/2}$ state and the radiative decay rates of the $2p_{1/2,3/2}$ states. The collision-induced transitions are dominated by proton impacts and the departure from the statistical ratios occurs because the rate coefficients for $2s_{1/2}$-$2p_{1/2}$ and $2s_{1/2}$-$2p_{3/2}$ transitions are very different in magnitude.

A simple formula may be derived that demonstrates the role of the proton collisions. The rate coefficients for transitions between $2p_{1/2}$ and $2p_{3/2}$ are small compared to the other transitions. Because the $2p_{1/2}$ and $2p_{3/2}$ levels decay rapidly by electron dipole radiation, we may at low density ignore the collisional transfer out of them. Thus if we designate the $2s_{1/2}$, $2p_{1/2}$, and $2p_{3/2}$ levels by the numbers 1, 2, and 3, respectively, we may put C_{23}, C_{32}, C_{21}, and C_{31} equal to zero. Then Eq. (38) can be solved to yield

$$\beta=\frac{1}{2}\left[\frac{1+\dfrac{rC_{12}}{(A_1/\eta)+C_{12}+C_{13}}}{1+\dfrac{rC_{13}/2}{(A_1/\eta)+C_{12}+C_{13}}}\right], \tag{39}$$

where r is the ratio $q_1/q_2=2q_1/q_3$. An expression of more general applicability has been given by Boiko, Pikuz, and Faenov.[23] At low temperatures, $C_{12}\gg C_{13}$ and we may further simplify (39) to the expression

$$\beta=\frac{1}{2}\left[1+\frac{rC_{12}}{(A_1/\eta)+C_{12}}\right]. \tag{40}$$

For Mg^{11+} the value of r is about 0.7 over a wide range of temperatures and

$$\beta\approx\frac{1}{2}\left[1+\frac{0.7}{1+A_1/\eta C_{12}}\right]. \tag{41}$$

These simple formulas fail at high densities.

Departures of β from 0.5 have been observed for Mg^{11+} in solar flares. Phillips *et al.*[1] measured a ratio of 0.64. To obtain such a ratio from Eq. (41) requires a density exceeding 10^{14} cm^{-3} which is 2 orders of magnitude larger than is plausible. Thus, although proton impacts can produce departures from 0.5, they are not responsible for the departures observed in solar flares. Ljepojevic *et al.*[6] have shown that the inclusion of contributions from the $2s_{1/2}$ magnetic dipole radiation and from satellite lines of heliumlike Mg^{10+} does not resolve the discrepancy and it appears that the assumption of an optically thin plasma in steady-state equilibrium must be discarded.

ACKNOWLEDGMENT

This work was supported by the U.S. Department of Energy, Office of Basic Energy Sciences, Division of Chemical Sciences.

[1] K. J. H. Phillips, J. W. Leibacher, C. J. Wolfson, J. H. Parkinson, B. C. Fawcett, B. J. Kent, H. E. Mason, L. W. Acton, J. L. Culhane, and A. H. Gabriel, Astrophys. J. **256**, 774 (1982).

[2] E. Källne, J. Källne, and J. E. Rice, Phys. Rev. Lett. **49**, 330 (1982).

[3] V. A. Boiko, A. V. Vinogradov, S. A. Pikuz, I. Yu. Skobelev, A. Ya. Faenov, and E. A. Yukov, Fiz. Plazmy Sov. J. Plasma Phys. **4**, 54 (1978).

[4] A. V. Vinogradov, I. Yu. Skobelev, and E. A. Yukov, Sov. J. Plasma Phys. **3**, 389 (1977).

[5] I. L. Beigman, L. A. Bureeva, and I. Yu. Skobelev, Sov. Astron. **23**, 725 (1979).

[6] N. N. Ljepojevic, R. J. Hutcheon, and R. W. P. McWhirter, J. Phys. B **17**, 3057 (1984); N. N. Ljepojevic, R. W. P. McWhirter, and S. Volonte, *ibid.* **18**, 3285 (1985).

[7] G. S. Tallents, Phys. Rev. A **29**, 3461 (1984).

[8] V. P. Shevelko, I. Yu. Skobelev, and A. V. Vinogradov, Phys. Scr. **16**, 123 (1977).

[9] A. Burgess, D. G. Hummer, and J. A. Tully, Philos. Trans. R. Soc. London **266**, 225 (1970).

[10] J. C. Weisheit, in *Applied Atomic Collision Physics*, edited by H. S. W. Massey, E. W. McDaniel, and B. Bederson (Academic, New York, 1984), Vol. 2, p. 441.

[11] B. L. Whitten, N. F. Lane, and J. C. Weisheit, Phys. Rev. A **29**, 945 (1984).

[12] A. de-Shalit and I. Talmi, *Nuclear Shell Theory* (Academic, New York, 1963).

[13] H. Bethe and E. E. Salpeter, *Quantum Mechanics of One and Two-Electron Atoms* (Academic, New York, 1957).

[14] *Handbook of Mathematical Functions*, Natl. Bur. Stand. (U.S.) (Appl. Math. Ser. No. 55), edited by M. Abramowtiz and I. A. Stegun (U.S. GPO, Washington, D.C., 1970).

[15] S. Bienstock, T. G. Heil, and A. Dalgarno, Phys. Rev. A **29**, 503 (1984).

[16] K. Alder, A. Bohr, T. Huus, B. Mottelson, and A. Winther, Rev. Mod. Phys. **28**, 432 (1956).

[17] G. W. Erickson, J. Phys. Chem. Ref. Data **6**, 831 (1977).

[18] M. E. Rose, *Relativistic Electron Theory* (Wiley, New York, 1961).

[19] K. F. Scheibner, J. C. Weisheit, and N. F. Lane, Phys. Rev. A **35**, 1252 (1987).

[20] A. Jacobs, J. Quant. Spectrosc. Radiat. Transfer **12**, 243 (1972). In this paper the author derives an expression for the low velocity, proton-ion inelastic collision cross section using the assumption that the cross section is proportional to the product of the proton wave functions before and after the collision. This incorrect assumption leads to an expression [Eq. (27) of this reference] that predicts much smaller cross sec-

tions in the low collision velocity region than Eq. (30).
[21]F. A. Parpia and W. R. Johnson, Phys. Rev. A **26**, 1142 (1982).
[22]D. H. Sampson and A. D. Parks, Astrophys. J. Suppl. Ser. **28**, 323 (1974); J. Phys. B **11**, 541 (1978).
[23]V. A. Boiko, S. A. Pikuz, A. Ya. Faenov, J. Phys. B **12**, 1889 (1979).